molecular pharmaceutics

ARTICLE

pubs.acs.org/molecularpharmaceutics

Indocyanine Green-Containing Nanostructure as Near Infrared Dual-Functional Targeting Probes for Optical Imaging and Photothermal Therapy

Xiaohui Zheng,[†] Da Xing,[*,†] Feifan Zhou,[†] Baoyan Wu,[†] and Wei R. Chen[†,‡]

[†]MOE Key Laboratory of Laser Life Science & Institute of Laser Life Science, College of Biophotonics, South China Normal University, Guangzhou 510631, China

[‡]Department of Engineering and Physics, College of Mathematics and Science, University of Central Oklahoma, Edmond, Oklahoma 73034, United States

ABSTRACT: Indocyanine green (ICG) is a near-infrared (NIR) imaging agent and is also an ideal light absorber for laser-mediated photothermal therapy. This NIR dye could serve as a basis of a dual-functional probe with integrated optical imaging and photothermal therapy capabilities. However, applications of ICG remain limited by its concentration-dependent aggregation, poor aqueous stability, nonspecific binding to proteins and lack of target specificity. To overcome these limitations, a novel ICG-containing nanostructure is designed utilizing the noncovalent self-assembly chemistry between phospholipid-polyethylene glycol (PL-PEG) and ICG. The interactions between both amphiphilic ICG and PL-PEG were studied using absorption and fluorescence spectroscopy. The properties of ICG-PL-PEG nanoprobe, such as absorption and fluorescence spectra, stability, morphology and size distribution, were also investigated. Two representative targeting molecules, namely, a small molecule, folic acid (FA), and a large protein, integrin $\alpha_v\beta_3$ monoclonal antibody (mAb), were conjugated to the surface of ICG-PL-PEG nanoprobe, displaying the diversity of ligand conjugation. The target specificity was confirmed using three cell lines with different levels of available folate receptors (FRs) or integrin $\alpha_v\beta_3$ expression via laser scanning confocal microscope and flow cytometry. This targeting ICG-PL-PEG nanoprobe could be internalized into targeted cells via ligand−receptor mediated endocytosis pathway. Our in vitro experiments showed that internalized ICG-PL-PEG could be used for cell imaging and selective photothermal cell destruction. These results represent the first demonstration of the dual functionality of ICG-containing nanostructure for targeted optical imaging and photothermal therapy of cancerous cells. This novel ICG-PL-PEG nanostructure, when conjugated with other therapeutic and imaging agents, could become a multifunctional probe for cancer diagnosis and treatment.

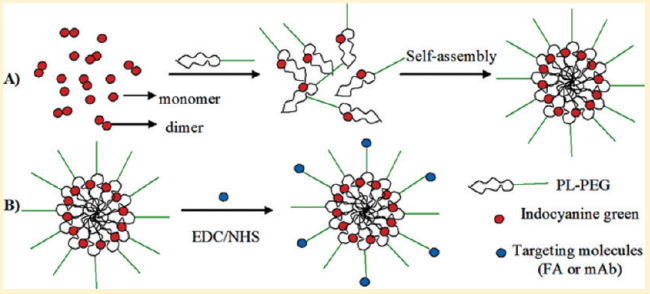

KEYWORDS: indocyanine green, phospholipid-polyethylene glycol, amphiphilic, self-assembly

INTRODUCTION

Optical imaging probes that use near-infrared (NIR) fluorophores offer several advantages over visible fluorophores, because living tissues display negligible absorption and autofluorescence in this NIR wavelength region.[1,2] Recently, photothermal therapy for cancers has been widely investigated as a minimally invasive treatment modality in comparison to other methods,[3,4] and the use of NIR light in the 700 to 1100 nm range for the photothermal interaction is particularly attractive.[5−8] Since both optical imaging and photothermal therapy require NIR probes, it is desirable to develop a dual-functional NIR probe. Indocyanine green (ICG) is currently the only Federal Drug Administration approved NIR clinical imaging agent[9−11] and is an ideal NIR light absorber for laser-mediated photothermal therapy.[12−16] Therefore, ICG is a suitable candidate for developing clinical NIR fluorescence imaging and photothermal therapy probes.

Several physicochemical characteristics, such as concentration-dependent aggregation, poor aqueous stability, nonspecific binding to proteins and lack of target specificity, have limited the applications of ICG. All these drawbacks lead to a fast degradation in aqueous media and quick clearance from the body with a short half-life about 2−4 min.[17−20] With such limitations, the use of ICG in optical imaging and photothermal therapy, as well as in molecular targeting, remains restricted. The utility of ICG for laser-mediated diagnostic and therapeutic applications could be greatly improved if ICG could preferentially accumulate at a targeted site in significant quantities.[21] Optical diagnosis or phototherapy requires extended laser exposure durations, up to several minutes. Therefore, it often requires several hours or even days to accumulate significant concentrations of the photosensitive agent in the target site after a systemic administration.

Received: September 2, 2010
Accepted: January 3, 2011
Revised: December 30, 2010
Published: January 03, 2011

ACS Publications © 2011 American Chemical Society

There are two approaches in directing nanostructures to hyperproliferative tissues such as tumor or inflammation tissues: passive targeting and active targeting. Passive targeting takes advantage of the inherent size of nanostructures and the unique properties of tumor vasculature such as the enhanced permeability and retention (EPR) effect, where the endothelial walls of tumor vasculature are characterized by enlarged pore size due to rapid angiogenesis and the lymph system around tumor grows too slowly to exclude foreign compounds from tumor region.[22−25] Active targeting, which is not only limited to hyperproliferative tissues, involves a ligand−receptor or antigen−antibody mediated endocytosis pathway.

It has been reported that nanostructures can improve the molecular instability of ICG or prolong its plasma half-life. For example, ICG-containing poly(lactic-*co*-glycolic acid) (PLGA) nanoparticles (>300 nm)[26,27] and nanoparticle-assembled capsules (NACs) (>400 nm)[28−30] showed increased stability and plasma half-life. However, both of these ICG-containing nanoparticles lie in the upper limit of the EPR effect. Oil in water emulsions containing ICG were found to show an increased blood half-life, but the stability was not examined.[31] Other inorganic delivery systems using silica nanoparticles and calcium phosphate nanoparticles have been developed, but these synthesis methods either involved multiple processing steps or used toxic organic and volatile solvents.[32,33] Preparation of micelles using a solvent evaporation method or a simple aqueous-based preparation method to encapsulate ICG was also investigated.[34,35] The size of micelles, approximately 10−100 nm, allows extravasation and permeation into tissues and yet is small enough to avoid clearance by the reticuloendothelial system (RES).[36,37] Prolonged circulation in the bloodstream is necessary to achieve a passive accumulation in tumors or sites of inflammation via the EPR effect. However, in these micelle drug delivery systems, a large amount of surfactants is required to stabilize and deliver a small amount of ICG, according to a mass ratio of 1:4000 or 1:10000, which may lyse cell membranes and denature proteins, and this approach therefore is not useful in biological environments. In addition, all these micelle carriers were based on the passive targeting approach, lacking the active targeting effect and photothermal capabilities.

Phospholipid micelles have been introduced as novel lipid based carriers for water insoluble drugs.[38,39] The self-assembled nanostructures of PEGylated phospholipids are attractive for ICG delivery because of multiple reasons. (1) This system, being composed of phospholipids and PEG, is biocompatible and relatively nontoxic. Phospholipids are the major component of cell membranes, and PEG has been approved for human use, therefore both of them are safe to use in biological systems. (2) As hydrophobic materials, phospholipid (PL) provides additional stability, because the existence of two hydrocarbon chains contributes considerably to the increased hydrophobic interactions,[40] which, in principle, can solubilize and stabilize a large amount of drug molecules per micelle. (3) The hydrophilic PEG surrounding the micelle surface renders the micelle sterically stable, protecting it from mononuclear phagocytic system (MPS) uptake and increasing drug circulation time.[41−43] (4) Both passive and active targeting can be realized, which will greatly increase drug accumulation in targeted tissues.

In this study, a novel ICG-containing nanostructure was developed utilizing the noncovalent self-assembly chemistry between phospholipid-polyethylene glycol (PL-PEG) and ICG. It takes only a few minutes for synthesis, and the processing occurs at room temperature and mild pH values in aqueous phase. The ICG within probes remains confined primarily to the network of PL by van der Waals forces. The interactions between both amphiphilic ICG and PL-PEG were studied using absorption and fluorescence spectroscopy. The properties of ICG-PL-PEG nanoprobe, such as absorption and fluorescence spectra, stability, morphology and size distribution, were also investigated. Two representative targeting molecules, namely, a small molecule, folic acid (FA), and a large protein, integrin $\alpha_v\beta_3$ monoclonal antibody (mAb), were conjugated to the surface of the ICG-PL-PEG nanoprobe, displaying the diversity of ligand conjugation. The target specificity was confirmed using three cell lines with different levels of available folate receptors or integrin $\alpha_v\beta_3$ expression. This targeting ICG-PL-PEG nanoprobe could be internalized by targeted cells via ligand−receptor mediated endocytosis pathway. Our in vitro experiments showed that internalized ICG-PL-PEG could be used for cell imaging and selective photothermal cell destruction. These results represent the first demonstration of the dual functionality of ICG-containing nanoprobe for targeted optical imaging and selective photothermal therapy of cancerous cells.

EXPERIMENTAL SECTION

Chemicals and Reagents. The following chemicals and reagents were used in our experiments: 1,2-distearoyl-*sn*-glycero-3-phosphoethanolamine-*N*-[amino/carboxy (polyethylene glycol) 2000] (PL-PEG-NH_2/COOH) (Avanti Polar Lipids Inc., Mt. Eden, AL, USA), indocyanine green for injection (Dan Dong Yi Chuang Company), CCK-8 (Dojindo Laboratories, Kumamoto, Japan), folic acid (Sigma, St. Louis, MO, USA), folic acid (FA) (Sigma, St. Louis, MO, USA), integrin $\alpha_v\beta_3$ (23C6) monoclonal antibody (integrin $\alpha_v\beta_3$ mAb) (Santa Cruz, CA, USA), folate receptor (FL-257) polyclonal antibody (Santa Cruz, CA, USA), *N*-hydroxysulfosuccinimide (NHS) and 1-ethyl-3-(3-(dimethylamino)propyl)carbodiimide (EDC) (Sigma-Aldrich Co). Since all the reagents were of analytical grade, they were used without further purification.

Preparation of ICG-PL-PEG Probe. The plain ICG-PL-PEG probe without adding targeting molecules was prepared using aqueous-based preparation method, in which PL-PEG was simply added to the distilled water at room temperature. A stock solution of ICG was also placed in distilled water. The probe was prepared by mixing the ICG and PL-PEG according to the mass ratio 1:100. The mixed solutions were stirred at room temperature for 5 min. Before preparing targeting ICG-PL-PEG probe, the solution was filtrated using 2000 Da filters (Millipore) to remove excess nonbinding ICG.

Preparation of Targeting ICG-PL-PEG Probe

Solution of PL-PEG-FA. FA solution was activated by EDC/NHS to afford FA-NHS (molar ratio, FA:EDC:NHS = 1:1:1). PL-PEG-FA was produced by incubating FA-NHS with PL-PEG-NH_2 (molar ratio, FA-NHS: PL-PEG-NH_2 = 2:1) (pH 7.4) for 4 h. After reaction, the solution was filtrated using 2000 Da filters (Millipore) to remove excess FA-NHS, EDC and NHS.

Solution of PL-PEG-mAb. PL-PEG-COOH solution was activated by EDC/NHS to afford PL-PEG-NHS (molar ratio, PL-PEG:EDC:NHS = 1:2:2). After reaction, the solution was dialyzed against PBS using a 2000 Da membrane (Millipore) to remove excessive EDC and NHS. To ensure complete removal, the dialysis lasted 3 to 4 days with frequent replacement of the PBS buffer. PL-PEG-mAb was produced by incubating integrin $\alpha_v\beta_3$ monoclonal antibody with PL-PEG-NHS (molar ratio, PL-PEG-NHS:integrin $\alpha_v\beta_3$ monoclonal antibody = 200:1) (pH 7.4) for 4 h.

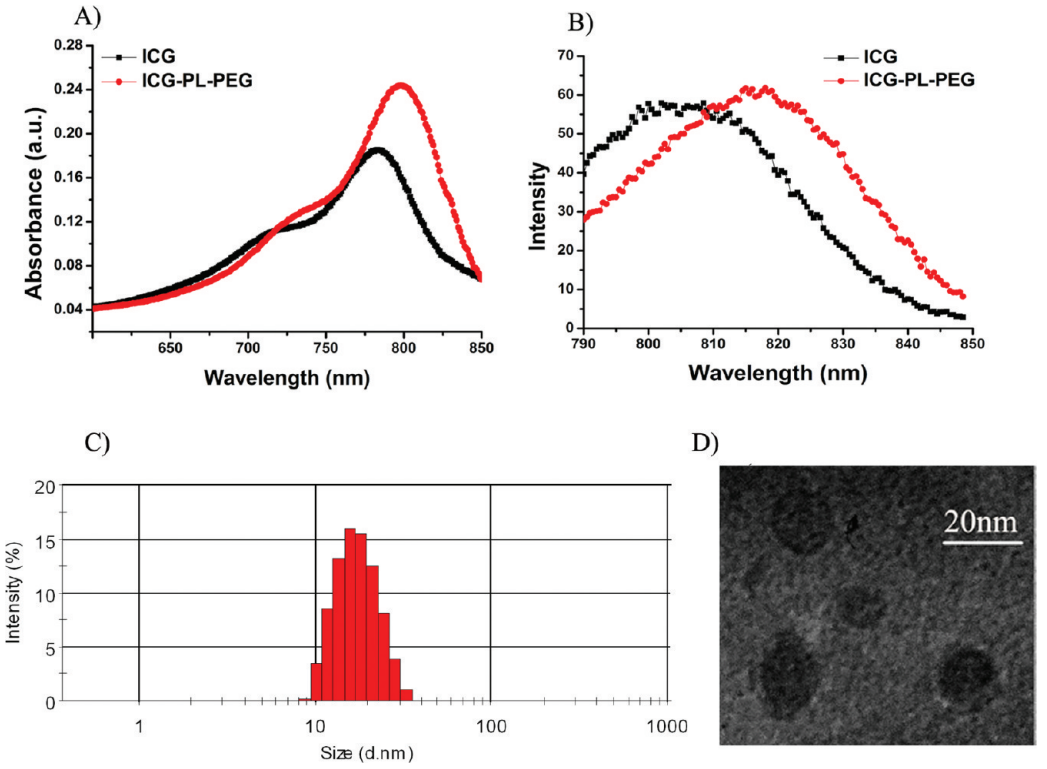

Figure 1. Absorption (A) and fluorescence (B) spectra of ICG and ICG-PL-PEG, respectively. Both peak absorption and peak emission of ICG-PL-PEG were in the near-infrared region and experienced a slight red shift. The morphology and size distribution of ICG-PL-PEG probes were measured using dynamic light scattering (DLS) (C) and transmission electron microscopy (TEM) imaging (D). The average diameter of the ICG-PL-PEG probe was 17.6 nm.

Optical Spectra Measurements. The absorption spectra of freely dissolved ICG and plain ICG-PL-PEG probe self-assembled by PL-PEG and ICG were obtained using a UV/vis spectrometer (Lambda 35, Perkin-Elmer, USA). Fluorescence spectra were obtained using an LS-55 fluorescence spectrophotometer (Perkin-Elmer, USA) with an excitation of 780 nm.

Dynamic Light Scattering (DLS) Measurement. The size and size distribution of ICG-PL-PEG probes were measured by dynamic light scattering (DLS) using a Malvern ZS90 equipped with a 532 nm laser beam and a scattering angle of 90°. The measurements were performed at 25 °C without further dilution of the samples. For each sample, size distribution measurement was performed for fifteen cycles per run.

Transmission Electron Microscopy (TEM). To further examine the morphology and size of the probe, a JEM-100CXII transmission electron microscope (TEM) with parameters of 100 kV voltage and 70 pA current was used. The distribution of diameters was determined by using TEM images of at least one hundred probes.

FR+ Cell and FR− EMT6 Tumor Cells. Murine mammary tumor line EMT6 cells were cultured in RPMI 1640 (GIBCO) supplemented with 15% fetal bovine serum (FBS), penicillin (100 units/mL), and streptomycin (100 μg/mL) in 5% CO_2, 95% air at 37 °C in a humidified incubator. FR+ EMT6 cells were obtained by passaging the cells for at least four times in the FA-free medium before use to ensure all FRs were available on the surface of the cells. FR− cells were harvested by culturing cells in medium with abundant FA to reduce the available free FRs on the cell surfaces.[6,8] These procedures ensured a very high level of available FRs on the FR+ cells and a very low level of available FRs on the FR− cells.

U87-MG Cell and MCF-7 Cell. U87-MG human glioblastoma cancer cells and MCF-7 human breast cancer cells were cultured in Eagle's minimal essential medium (EMEM) and Dulbecco's modified Eagle's medium (DMEM), respectively. The media were supplemented with 10% fetal bovine serum (FBS) and 1% penicillin−streptomycin in 5% CO_2, 95% air at 37 °C in a humidified incubator. U87-MG cancer cells overexpress integrin $\alpha_v\beta_3$ on the cell surface while MCF-7 cancer cells express a very low level of integrin $\alpha_v\beta_3$.[44]

Selective Imaging of Cancer Cells. Different types of cancer cells (1×10^4 per well) growing in 35 mm Petri dishes were incubated with the targeting ICG-PL-PEG probe solution at 0.01 mg/mL ICG (mass ratio ICG:PL-PEG = 1:100) for 1 h, rinsed with PBS and replaced with fresh cell medium. The cells were imaged by a commercial laser scanning microscope (LSM 510/ConfoCor 2) combination system (Zeiss, Jena, Germany) equipped with a Plan-Neofluar 40×/1.3 NA Oil DIC objective. The targeting probe was excited at 633 nm, and its fluorescence emission was recorded through an LP650 nm filter.

Quantification of Fluorescence Intensity. To quantitatively assess fluorescence intensity, tumor cells were incubated with targeting probe solution in a 12-well microplate for 1 h, rinsed with PBS and then harvested with trypsin. Different types of cells were washed and resuspended in ice-cold PBS. The fluorescence histogram of cells in different treatments was obtained from 10,000 cells by flow cytometry (Becton Dickinson FACScan).

Temperature Measurement and Selective Killing of Cancer Cells during NIR Irradiation. ICG-PL-PEG solution of different concentrations was irradiated by the 808 nm laser at 1.25 W/cm^2. Temperature was measured in 10 s intervals with a

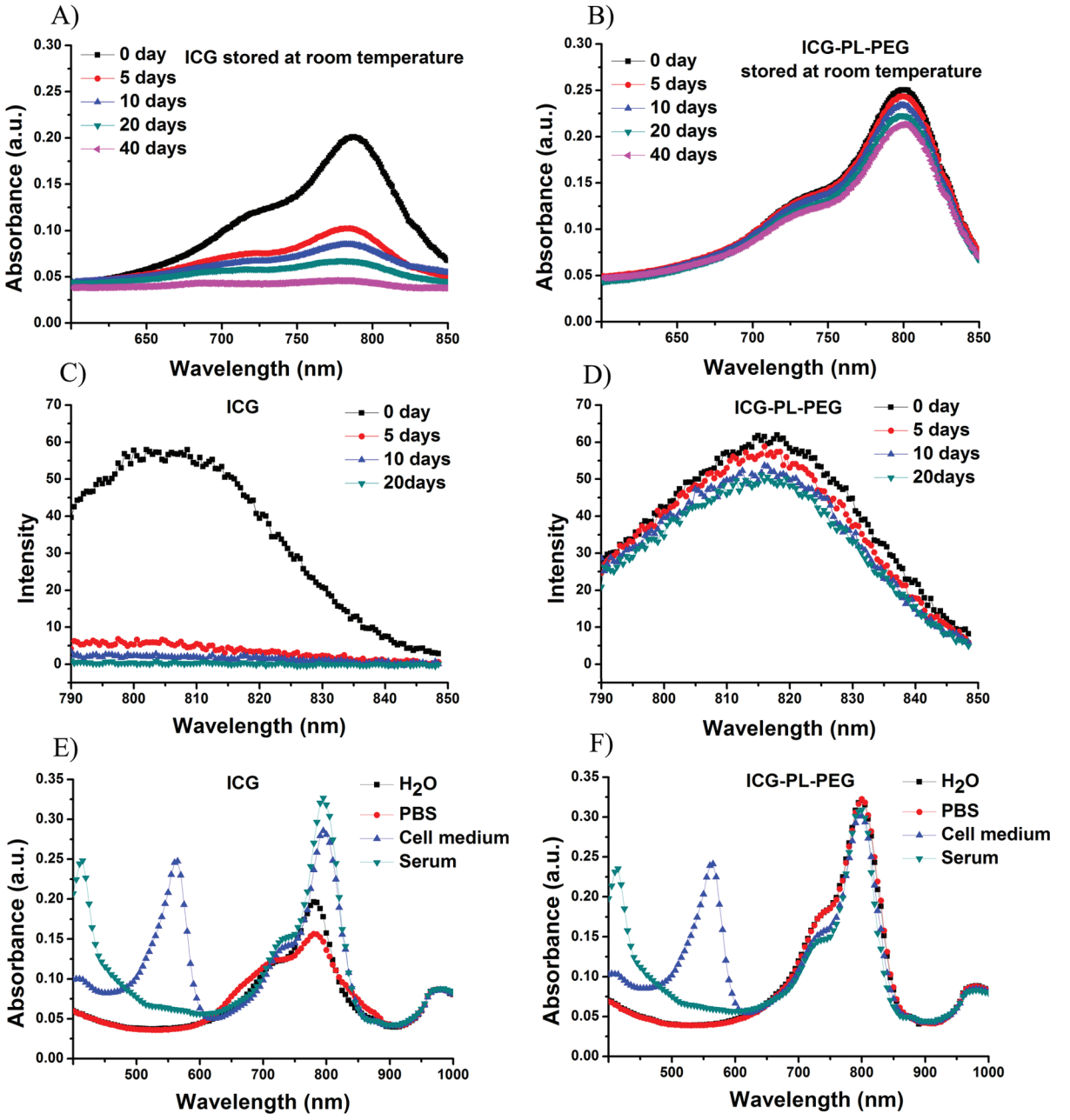

Figure 2. Absorption and fluorescence spectra of ICG (A and C) and ICG-PL-PEG probe (B and D) at different times. Absorption spectra of ICG (E) and ICG-PL-PEG (F) probe in four different biorelevant solvents. The results demonstrated the probe had a high stability compared to freely dissolved ICG.

thermocouple placed inside the solution for a total of 2 min. The thermocouple was placed outside the path of the laser beam to avoid direct exposure of the thermocouple to the laser light.

Different types of cancer cells (1×10^4 per well) growing in 35 mm Petri dishes were incubated with the targeting ICG-PL-PEG probe solution at 0.01 mg/mL ICG (mass ratio ICG:PL-PEG = 1:100) for 1 h, rinsed with PBS and replaced with fresh cell medium. Then all cancer cells were exposed to light at a fluence of 1.25 W/cm^2 for 5 min. After being cultured for another 4 h, different types of cancer cells were observed using an optical microscope.

Quantification of Photothermal Effect. To quantitatively assess photothermal cytotoxicity, tumor cells were incubated with targeting probe solution in a 96-well microplate for 1 h and rinsed with PBS. Different laser irradiation power densities were obtained by changing the output power with a fixed laser spot. Tumor cells were irradiated with a power density ranging from 0.75 to 3.25 W/cm^2 for 5 min. Cell cytotoxicity was assessed 12 h after the laser irradiation with CCK-8. OD450, the absorbance value at 450 nm, was read with a 96-well plate reader (INFINITE M200, Tecan, Switzerland), to determine the viability of the cells.

RESULTS

Characterization of Freely Dissolved ICG and ICG-PL-PEG Probe. To analyze the optical properties of freely dissolved ICG and ICG-PL-PEG probe, 5 mg/L ICG was used for both

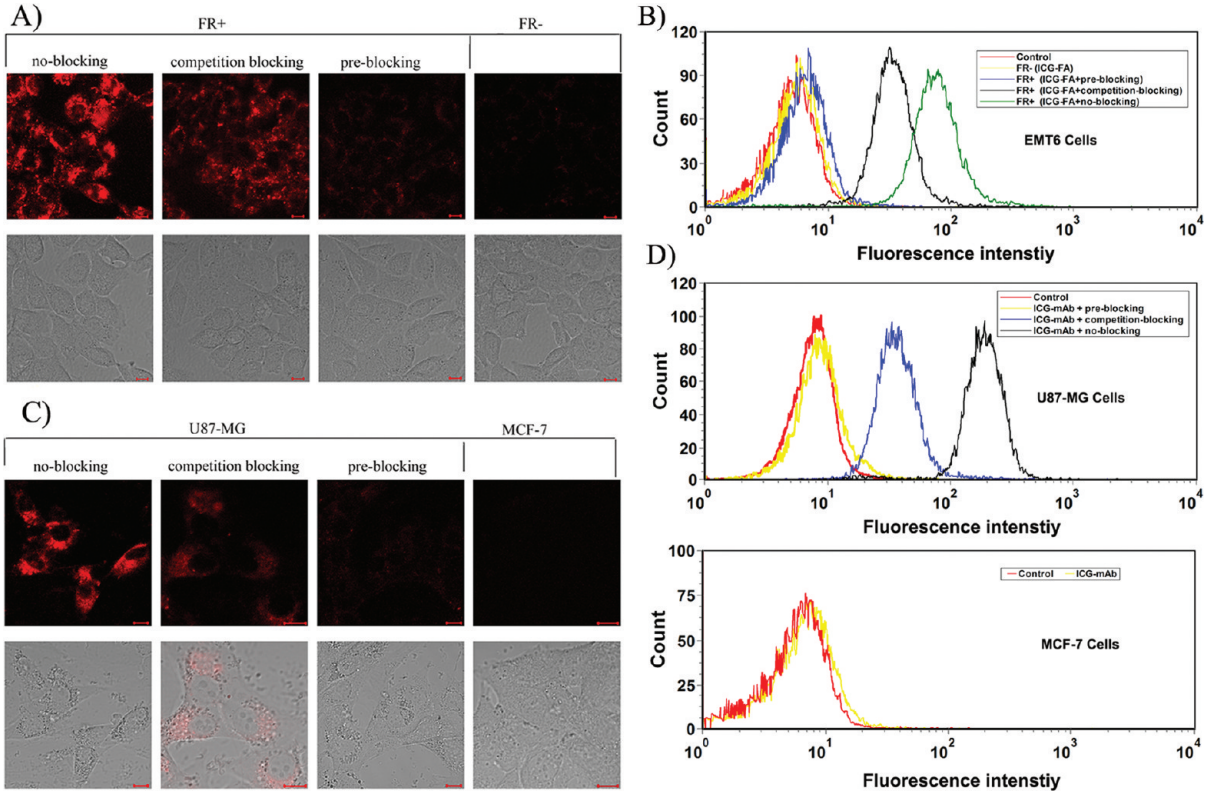

Figure 3. (A) Confocal images and (B) fluorescence histograms of EMT6 cells after incubation in a solution of the targeting ICG-PL-PEG probe conjugated with FA under different treatments (abbreviated as ICG-FA). FR+ EMT6 cells were obtained by passaging the cells for at least four times in the FA-free medium before use to ensure all FRs were available on the surface of the cells. FR− cells were harvested by culturing cells in medium with abundant FA to reduce the available free FRs on the cell surfaces. (C) Confocal images and (D) fluorescence histograms of integrin positive cells (U87-MG) and integrin negative cells (MCF-7) after incubation in a solution of the targeting ICG-PL-PEG probe conjugated with integrin $\alpha_v\beta_3$ mAb under different treatments (abbreviated as ICG-mAb). Bar: 10 μm.

solutions, at which no quenching effect of the dye occurred. The required PL-PEG concentration was determined as 0.5 mg/mL by absorption and fluorescence spectra, at which no more shifts in the peak absorption and peak emission occurred. At the same time, there was no fluorescence quenching. The mass ratio of ICG and PL-PEG was 1:100. At this concentration, PL-PEG as a typical amphiphilic molecule was found to form polymeric micelles in an aqueous environment. Compared to freely dissolved ICG, the absorption and emission spectra of the ICG-PL-PEG probe were red-shifted by approximately 20 nm and 15 nm, respectively (Figure 1A and Figure 1B). The average diameter of the ICG-PL-PEG probe was 17.6 nm, which was demonstrated both by dynamic light scattering and by transmission electron microscopy (Figure 1C and Figure 1D).

Stability of Freely Dissolved ICG and ICG-PL-PEG Probe. To determine whether the probe had a higher stability than freely dissolved ICG, absorption spectra of the ICG and ICG-PL-PEG probe were measured at different times and in different aqueous solutions. The samples were maintained at 4 °C (data not shown) and room temperature without light exposure. We measured the absorbance of the samples continuously until freely dissolved ICG was almost completely degraded (Figure 2A). However, the ICG-PL-PEG probe only experienced a slight reduction of absorbance after 40 days (Figure 2B). Similarly, the emission intensity of aqueous ICG completely vanished after 20 days (Figure 2C) while slight reduction in fluorescence intensity of the PL-PEG-ICG probe was observed (Figure 2D). These two experiments fully demonstrated the stability of the ICG-PL-PEG probe.

In order to further determine whether the probe could have a higher stability against buffer conditions than ICG, we measured the absorption spectra of freely dissolved ICG and the ICG-PL-PEG probe in four different biorelevant solvents: H_2O, phosphate buffered solution (PBS), DMEM cell medium, and serum. The spectrum of freely dissolved ICG changed greatly in different media (Figure 2E) while the absorption spectrum of the ICG-PL-PEG probe showed no apparent change in any of the four biorelevant media (Figure 2F).

Selective Imaging of Cancer Cells with Targeting ICG-PL-PEG Probe. To examine the characteristics of the probe as a cancer-targeting fluorescent probe, optical imaging experiments were performed. In order to target cancer cells, FA or mAb was used with different cell lines. The FR positive EMT6 cells (FR+ cells), with all available folate receptors (FRs) on cell surface, and the FR negative EMT6 cells (FR− cells), with few available FRs, were used. U87-MG cells with overexpressed integrin $\alpha_v\beta_3$ and MCF-7 cells with few integrin $\alpha_v\beta_3$ were also used. The results showed that, in the cell lines with excessive receptors, such as FRs (Figure 3A) and integrin $\alpha_v\beta_3$ (Figure 3C), the fluorescence intensity of ICG was much higher than that in the cell lines with few receptors on the surface. In order to further confirm the target specificity, blocking experiments by adding receptors directed antibodies (Ab) with the targeting probes to the cell solutions were conducted. The fluorescence intensity of FR+ cells in

dx.doi.org/10.1021/mp100301t |*Mol. Pharmaceutics* 2011, 8, 447–456

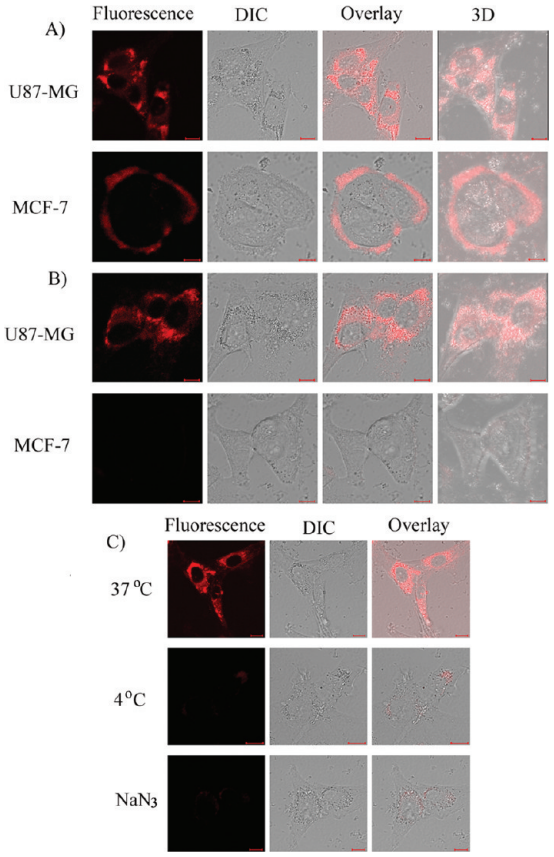

Figure 4. (A) Confocal images of U87-MG and MCF-7 cells after incubation with targeting ICG-PL-PEG probe before being washed by PBS. (B) Confocal images of U87-MG and MCF-7 cells after incubation with targeting ICG-PL-PEG probe after being washed by PBS. (C) Confocal images of U87-MG cells after incubation with targeting probe at 37 °C, 4 °C and pretreated with NaN_3 at 37 °C. Bar: 10 μm.

no-blocking, competition-blocking (the Ab and targeting probes were added simultaneously) and preblocking settings showed a gradient of decrease (Figure 3A). Such decrease was further demonstrated by fluorescence histograms obtained by flow cytometry (Figure 3B). In the preblocking setting, the fluorescence intensity was almost the same as that of FR− cells (cultured with abundant FA to remove all available FRs), and was only slightly higher than that of the control groups (without incubation with targeting probe solution). The similar results were obtained in the integrin experiments (Figure 3C and Figure 3D).

It is believed that targeting probe was mainly internalized into cells via ligand−receptor or antigen−antibody mediated endocytosis pathway. To further confirm this hypothesis, we observed the interactions of targeting probe with integrin positive cells (U87-MG) and integrin negative cells (MCF-7). Before being washed by PBS, the fluorescence emission from the U87-MG cells indicated the uptake of the targeting probe; however, the fluorescence emission from only the surface of MCF-7 cells indicated the absence of uptake of the targeting probe (Figure 4A). After being washed by PBS, the fluorescence emission from U87-MG cells remained the same, while the fluorescence emission from the surface of MCF-7 cells disappeared (Figure 4B). Endocytosis is usually prohibited when incubations are carried out at low temperature (4 °C instead of 37 °C) or in ATP (adenosine triphosphate) depleted environments such as pretreated with NaN_3.[45,46] In our experiments, U87-MG cells were incubated with the targeting probe at 37 °C or 4 °C, or pretreated with NaN_3 (10 mM) at 37 °C. The fluorescence images of the cells after these different treatments were acquired (Figure 4C). Apparently, these images demonstrated that the incubation at 4 °C and pretreatment with NaN_3 at 37 °C both inhibited the endocytosis pathway. These two experiments confirmed our hypothesis of the endocytosis mechanism.

Selective Killing of Cancer Cells with Targeting ICG-PL-PEG Probe. For photothermal treatment of cancer cells, we measured the temperature increase in ICG-PL-PEG solutions of different concentrations. At an irradiation power density of 1.25 W/cm^2, the temperature increased rapidly in the first 30 s and gradually reached a plateau after 1 min (Figure 5A). In the absence of ICG-PL-PEG probe, the temperature only increased by 2−3 °C, indicating that laser irradiation at this power density caused minimal thermal effect. In the presence of 0.0005 mg/mL ICG (0.65 μM), the temperature increased by 5−10 °C. Such a change could increase temperature from 37 °C to >42 °C, leading to an irreversible damage to cells.

To examine the characteristics of the targeting probe as a specific photothermal therapy probe, an optical microscope was used. Cancer cells were incubated with the targeting probe solution for 1 h, washed and then irradiated with an 808 nm laser at 1.25 W/cm^2 for 5 min. After irradiation, extensive cell death was observed only in the targeted cancer cells (FR+ EMT6 cells and U87-MG cells), evidenced by drastic cell morphology changes (Figure 5B, right column), but the cells without incubating with the targeting probe remained intact under laser irradiation (Figure 5B, left column). FR− EMT6 cells cells and MCF-7 cells with few available FR or integrin $\alpha_v\beta_3$ expressions had no apparent change under these two treatments.

Under a laser influence of 1.25 W/cm^2 for 5 min, the viability of FR− cells treated by the targeting probe solution showed no apparent change compared to control, but the viability of FR+ cancer cells decreased by 25−40%. No apparent decrease of cell viability was observed when cells were treated by the targeting probe without laser irradiation or treated only by the laser. These results suggested that FR+ cancer cells could selectively internalize the targeting probe and could be selectively killed by irradiation by the 808 nm laser while FR− cells were not affected by the targeting ICG-PL-PEG probe. Similar results were obtained in integrin $\alpha_v\beta_3$ experiments; however, cell viability of U87-MG cancer cells decreased by 35−55%.

To study thermal toxicity, tumor cells were irradiated by laser with a power density ranging from 0.75 to 3.25 W/cm^2 with or without the presence of the probe. For all cases, cells retained their viability when irradiated by laser alone. When ICG-PL-PEG was used, cell viability decreased significantly under laser irradiation, as shown in Figure 5D. A 75% cell lethality was reached with a power density of 2.75 W/cm^2 and 2.25 W/cm^2 on FR+ cells and U87-MG cells, respectively. This minor difference may be due to different amounts of targeting probes internalized into cancer cells and due to different heat resistances between FR+ and U87-MG cells.

DISCUSSION

Concentration-dependent aggregation is a well-known phenomenon for ICG in aqueous solution. The amphiphilic character of ICG leads to self-organization into highly ordered aggregates predominantly caused by van der Waals forces and hydrophobic interactions.[10] The dye−dye interactions have adverse effects

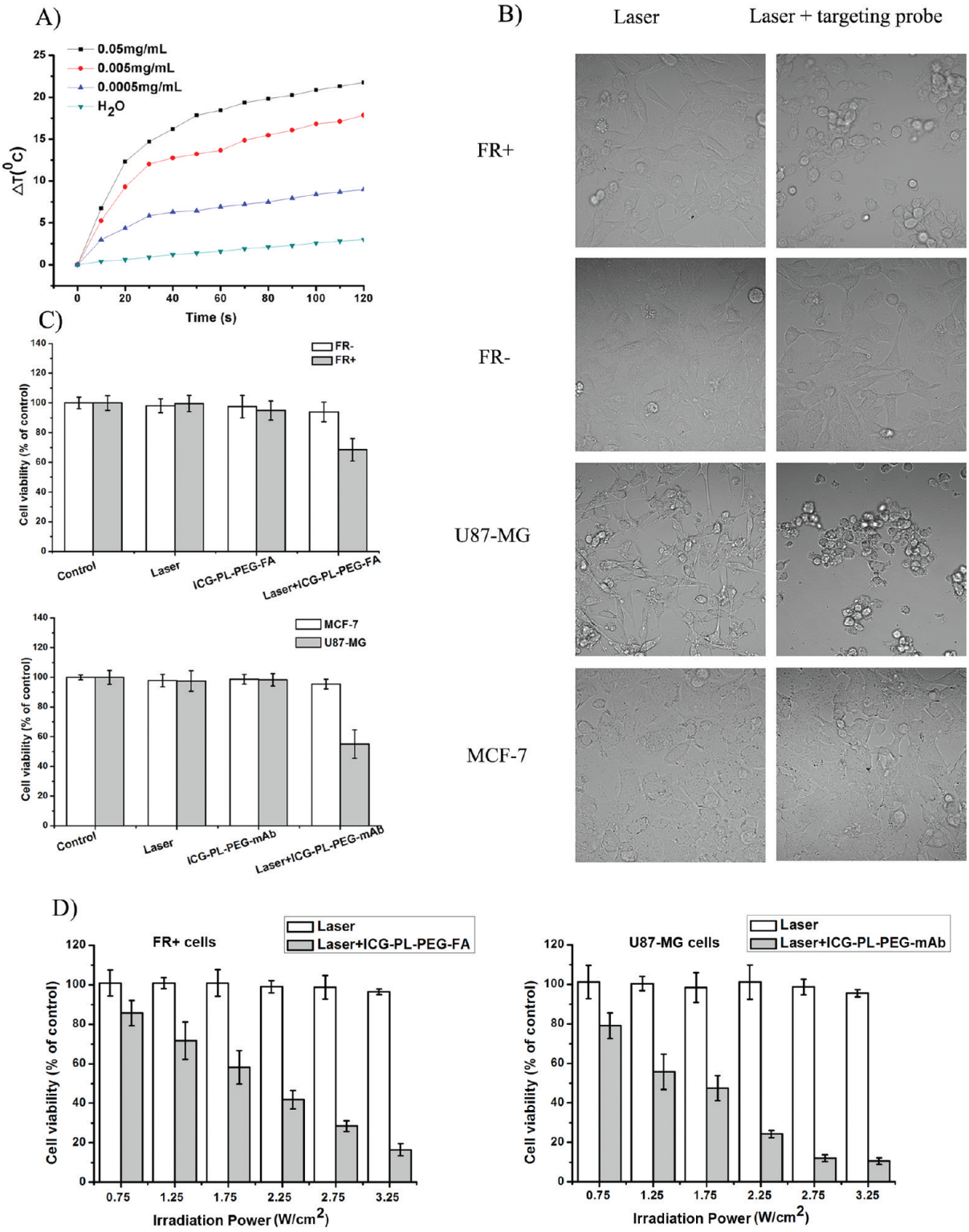

Figure 5. (A) Temperature increase in ICG-PL-PEG solutions of different concentrations under laser irradiation. (B) Optical images of different cancer cells under different treatments. FR+ EMT6 cells and U87-MG cells remained unharmed under laser irradiation (808 nm laser at 1.25 W/cm^2 for 5 min) without probe (left column). Extensive cell death was observed under laser irradiation after tumor cells were incubated with targeting ICG-PL-PEG probe (right column). FR− EMT6 cells and MCF-7 cells with few available FRs or integrin $\alpha_v\beta_3$ had no apparent change under these two treatments. (C) Quantification of photothermal effect on cancer cell killing under different treatments. Only targeted cancer cells showed an apparent decrease of viability. Bars, means ± SD (n = 6). (D) Cell viability of target cells was assessed after NIR laser irradiation with different irradiation power densities for 5 min. Bars, means ± SD (n = 4).

dx.doi.org/10.1021/mp100301t |*Mol. Pharmaceutics* 2011, 8, 447–456

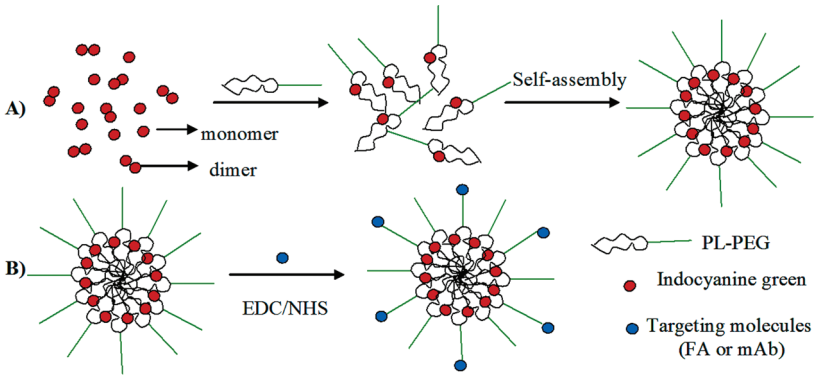

Figure 6. (A) Self-assembly process of ICG-PL-PEG probe. (B) Targeted modification of ICG-PL-PEG probe. FA or mAb was linked on the surface via amidation reaction. EDC: 1-ethyl-3-(3-(dimethylamino)propyl)carbodiimide. NHS: *N*-hydroxysulfosuccinimide.

on the optical properties, such as lower quantum yields due to self-quenching and spectral changes due to forming dimers or J-aggregates.[35] In our experiment, the ratio of monomer to dimer in ICG solution was respectively 1.5 and 1.1 at concentrations of 0.02 mg/mL and 0.05 mg/mL. After adding PL-PEG according to the mass ratio of 1:100, the ratio of monomer to dimer changed to 2.5 and 2.0 respectively at the same ICG concentration, indicating that the noncovalent binding between ICG and PL-PEG was a strong competition to self-aggregation between ICG and ICG. It is hypothesized that, due to the existence of two fatty acid acyls, PL-PEG contributes considerably to an increase in the van der Waals forces and hydrophobic interactions, which surpass the interactions between ICG itself. The binding site of ICG and PL-PEG is the PL portion, because the interactions between PL-PEG-COOH and PL-PEG-NH_2 have similar results. Furthermore, binding with PL has been reported[17,19,20] and some experiments have demonstrated that, in human blood, most of ICG would bind to high-density lipoprotein (HDL) and low-density lipoprotein (LDL) due to the same lipid components. Experiments further demonstrated that, when aqueous ICG was mixed with different types of lipids existing in human plasma, such as free cholesterol, esterified cholesterol, triacylglycerol, and phospholipid (PL), almost all ICG would bind to PL.[17]

Previous studies showed that stability of ICG encapsulated in various carriers can be increased,[26,27,29] but only up to a period of 3−5 days. Use of a micelle system allowed a higher stability to be obtained,[34,35,47] among which encapsulation within Solutol HS 15 micelles preserved the initial absorbance of ICG even at room temperature after 4 weeks, which demonstrated a superior stabilization. However, in this micelle system, to stabilize a certain amount of ICG, a large amount of HS 15 was used, about 1:10000 according to mass ratio, which may lyse cell membranes and denature proteins. The investigations in the present study exhibited similar stability as encapsulation within Solutol HS 15 micelles, but the mass ratio was only 1:100. Therefore it greatly decreased the amount of polymer molecules. Comparing the chemical structure of Solutol HS 15 and PL, PL has two fatty acid acyls while Solutol HS 15 has one. However, to stabilize the same amount of ICG, the amount of PL-PEG required is only 1/100 of Solutol HS 15. It is apparent that the two chains of the fatty acid acyls significantly increased the van der Waals force between ICG and PL-PEG and enhanced the hydrophobicity. Such strong binding resulted in the stability of ICG in the nanocarriers like PL-PEG.

Targeted conjugates that employ cell type-specific binding by ligand−receptor or antibody−antigen recognition provide higher selectivity. However, when ICG was directly attached to monoclonal antibody (mAb) via hydrophobic interactions or van der Waals force, ICG dramatically lost its fluorescence.[48−50] Some targeting ligands with a low molecular weight such as FA cannot be directly attached to ICG due to its amphiphilicity and lack of functional groups. However, ICG-PL-PEG nanostructure can be surface-modified with either a small molecule (such as folic acid) or a large protein (such as integrin $\alpha_v\beta_3$ monoclonal antibody). Furthermore, the use of a certain amount of targeting molecules does not affect the integrity and properties of ICG-PL-PEG nanoprobe. Selectively imaging and photothermal therapy of cancer cells can be realized using this novel ICG-PL-PEG nanoprobe.

Based on the characteristics of ICG-PL-PEG, it is expected that the self-assembly process of this probe follows the scheme outlined in Figure 6. In summary, noncovalent binding between ICG and PL-PEG was a strong competition to self-aggregation between ICG and ICG due to the existence of two fatty acid acyls. PL-PEG as a typical amphiphilic molecule was found to form polymeric micelles in aqueous environment. All these were self-assembly processes. Then targeting molecules such as FA or mAb were linked at the terminal of PEG by amidation reaction. Based on this novel ICG-PL-PEG nanostructure, a multifunctional probe for cancer diagnosis and treatment could be developed when conjugated with other therapeutic and imaging agents.

The development of dual-functional even multifunctional probes is necessary in treating cancers, and it has been attracting more and more attention in recent years. Coupling a biomedical imaging application to a cancer therapy application would potentially yield significant effect on cancer treatment. Gold nanorod and nanoshell integrated dark-field light scattering imaging and photothermal therapy have been investigated.[5,7] Single walled carbon nanotubes have also been investigated as near-infrared agents for fluorescence imaging and cancer cell destruction.[8,51] According to the parameter of optical absorption divided by weight, ICG is 7 times more efficient than SWNTs and ∼8500 times more efficient than commercial gold nanorods with a peak absorption at 780 nm.[52] Previous studies showed that, by in situ injection method, near-infrared laser irradiation conjugated with ICG can cause apparent photothermal interaction with tumor tissues and achieve a significant inhibition on tumor growth.[12−16] It is expected that early diagnosis and treatment of cancers can be achieved using ICG-PL-PEG nanoprobe, which is based on greatly improving the efficiency of both passive and active targeting.

ICG-PL-PEG can be used as an agent to monitor the effect of photothermal treatment, and it can also be a basis for development of multifunctional probes after being conjugated with other imaging and therapy agents such as magnetic beads or chemotherapy drugs.

CONCLUSION

In summary, we have reported a novel ICG-PL-PEG probe with several unique features. It has a highly stable structure and functionality in light absorption and fluorescence. Furthermore, its absorption and emission peaks are in the NIR range. Its components are nontoxic. Further modification of this probe with targeting agents can render it a great potential for optical imaging and selective phototherapy.

AUTHOR INFORMATION

Corresponding Author

*D.X.: South China Normal University, MOE Key Laboratory of Laser Life Science, Institute of Laser Life Science, Guangzhou 510631, China; tel, (+86-20) 8521-0089; fax, (+86-20) 8521-6052; e-mail, xingda@scnu.edu.cn.

ACKNOWLEDGMENT

This research is supported by the National Basic Research Program of China (2010CB732602; 2011CB910402), the Program for Changjiang Scholars and Innovative Research Team in University (IRT0829), the National Natural Science Foundation of China (30870676; 30800261), and the US National Institutes of Health (P20 RR016478 from the INBRE Program of the National Center for Research Resources).

REFERENCES

(1) Sharma, R.; Wendt, J. A.; Rasmussen, J. C.; Adams, K. E.; Marshall, M. V.; Sevick-Muraca, E. M. New horizons for imaging lymphatic function. *Ann. N.Y. Acad. Sci.* **2008**, *1131*, 13–36.

(2) Weissleder, R. A clearer vision for in vivo imaging. *Nat. Biotechnol.* **2001**, *19*, 316–317.

(3) Amin, Z.; Donald, J. J.; Masters, A.; Kant, R.; Steger, A. C.; Bown, S. G.; Lees, W. R. Hepatic metastases: interstitial laser photocoagulation with real-time US monitoring and dynamic CT evaluation of treatment. *Radiology* **1993**, *187*, 339–347.

(4) Nolsoe, C. P.; Torp-Pedersen, S.; Burcharth, F.; Horn, T.; Pedersen, S.; Christensen, N. E.; Olldag, E. S.; Andersen, P. H.; Karstrup, S.; Lorentzen, T. Interstitial hyperthermia of colorectal liver metastases with a US-guided Nd-YAG laser with a diffuser tip: a pilot clinical study. *Radiology* **1993**, *187*, 333–337.

(5) Huang, X.; El-Sayed, I. H.; Qian, W.; El-Sayed, M. A. Cancer cell imaging and photothermal therapy in the near-infrared region by using gold nanorods. *J. Am. Chem. Soc.* **2006**, *128*, 2115–2120.

(6) Zhou, F.; Xing, D.; Ou, Z.; Wu, B.; Resasco, D. E.; Chen, W. R. Cancer photothermal therapy in the near-infrared region by using single-walled carbon nanotubes. *J. Biomed. Opt.* **2009**, *14*, 021009.

(7) Loo, C.; Lowery, A.; Halas, N.; West, J.; Drezek, R. Immunotargeted nanoshells for integrated cancer imaging and therapy. *Nano Lett.* **2005**, *5*, 709–711.

(8) Kam, N. W.; O'Connell, M.; Wisdom, J. A.; Dai, H. Carbon nanotubes as multifunctional biological transporters and near-infrared agents for selective cancer cell destruction. *Proc. Natl. Acad. Sci. U.S.A.* **2005**, *102*, 11600–11605.

(9) Sakka, S. G. Assessing liver function. *Curr. Opin. Crit. Care* **2007**, *13*, 207–214.

(10) Landsman, M. L.; Kwant, G.; Mook, G. A.; Zijlstra, W. G. Light-absorbing properties, stability, and spectral stabilization of indocyanine green. *J. Appl. Physiol.* **1976**, *40*, 575–583.

(11) Dzurinko, V. L.; Gurwood, A. S.; Price, J. R. Intravenous and indocyanine green angiography. *Optometry* **2004**, *75*, 743–755.

(12) Chen, W. R.; Adams, R. L.; Bartels, K. E.; Nordquist, R. E. Chromophore-enhanced in vivo tumor cell destruction using an 808-nm diode laser. *Cancer Lett.* **1995**, *94*, 125–131.

(13) Chen, W. R.; Adams, R. L.; Heaton, S.; Dickey, D. T.; Bartels, K. E.; Nordquist, R. E. Chromophore-enhanced laser-tumor tissue photothermal interaction using an 808-nm diode laser. *Cancer Lett.* **1995**, *88*, 15–19.

(14) Chen, W. R.; Adams, R. L.; Higgins, A. K.; Bartels, K. E.; Nordquist, R. E. Photothermal effects on murine mammary tumors using indocyanine green and an 808-nm diode laser: an in vivo efficacy study. *Cancer Lett.* **1996**, *98*, 169–173.

(15) Chen, W. R.; Liu, H.; Ritchey, J. W.; Bartels, K. E.; Lucroy, M. D.; Nordquist, R. E. Effect of different components of laser immunotherapy in treatment of metastatic tumors in rats. *Cancer Res.* **2002**, *62*, 4295–4299.

(16) Chen, W. R.; Singhal, A. K.; Liu, H.; Nordquist, R. E. Antitumor immunity induced by laser immunotherapy and its adoptive transfer. *Cancer Res.* **2001**, *61*, 459–461.

(17) Yoneya, S.; Saito, T.; Komatsu, Y.; Koyama, I.; Takahashi, K.; Duvoll-Young, J. Binding properties of indocyanine green in human blood. *Invest. Ophthalmol. Visual Sci.* **1998**, *39*, 1286–1290.

(18) Saxena, V.; Sadoqi, M.; Shao, J. Degradation kinetics of indocyanine green in aqueous solution. *J. Pharm. Sci.* **2003**, *92*, 2090–2097.

(19) Mordon, S.; Devoisselle, J. M.; Soulie-Begu, S.; Desmettre, T. Indocyanine green: physicochemical factors affecting its fluorescence in vivo. *Microvasc. Res.* **1998**, *55*, 146–152.

(20) Desmettre, T.; Devoisselle, J. M.; Mordon, S. Fluorescence properties and metabolic features of indocyanine green (ICG) as related to angiography. *Surv. Ophthalmol.* **2000**, *45*, 15–27.

(21) Yaseen, M. A.; Yu, J.; Jung, B.; Wong, M. S.; Anvari, B. Biodistribution of encapsulated indocyanine green in healthy mice. *Mol. Pharmaceutics* **2009**, *6*, 1321–1332.

(22) Brannon-Peppas, L.; Blanchette, J. O. Nanoparticle and targeted systems for cancer therapy. *Adv. Drug Delivery Rev.* **2004**, *56*, 1649–1659.

(23) Yuan, F.; Dellian, M.; Fukumura, D.; Leunig, M.; Berk, D. A.; Torchilin, V. P.; Jain, R. K. Vascular permeability in a human tumor xenograft: molecular size dependence and cutoff size. *Cancer Res.* **1995**, *55*, 3752–3756.

(24) Hobbs, S. K.; Monsky, W. L.; Yuan, F.; Roberts, W. G.; Griffith, L.; Torchilin, V. P.; Jain, R. K. Regulation of transport pathways in tumor vessels: role of tumor type and microenvironment. *Proc. Natl. Acad. Sci. U.S.A.* **1998**, *95*, 4607–4612.

(25) Allen, T. M.; Cullis, P. R. Drug delivery systems: entering the mainstream. *Science* **2004**, *303*, 1818–1822.

(26) Saxena, V.; Sadoqi, M.; Shao, J. Enhanced photo-stability, thermal-stability and aqueous-stability of indocyanine green in polymeric nanoparticulate systems. *J. Photochem. Photobiol., B* **2004**, *74*, 29–38.

(27) Saxena, V.; Sadoqi, M.; Shao, J. Indocyanine green-loaded biodegradable nanoparticles: preparation, physicochemical characterization and in vitro release. *Int. J. Pharm.* **2004**, *278*, 293–301.

(28) Yaseen, M. A.; Yu, J.; Wong, M. S.; Anvari, B. Laser-induced heating of dextran-coated mesocapsules containing indocyanine green. *Biotechnol. Prog.* **2007**, *23*, 1431–1440.

(29) Yaseen, M. A.; Yu, J.; Wong, M. S.; Anvari, B. Stability assessment of indocyanine green within dextran-coated mesocapsules by absorbance spectroscopy. *J. Biomed. Opt.* **2007**, *12*, 064031.

(30) Yu, J.; Yaseen, M. A.; Anvari, B.; Wong, M. S. Synthesis of Near-Infrared-Absorbing Nanoparticle-Assembled Capsules. *Chem. Mater.* **2007**, *19*, 1277–1284.

(31) Devoisselle, J. M.; Soulie-Begu, S.; Mordon, S.; Desmettre, T.; Maillols, H. A Preliminary Study of the In Vivo Behaviour of an Emulsion Formulation of Indocyanine Green. *Lasers Med. Sci.* **1998**, *13*, 279–282.

(32) Altinoglu, E. I.; Russin, T. J.; Kaiser, J. M.; Barth, B. M.; Eklund, P. C.; Kester, M.; Adair, J. H. Near-infrared emitting fluorophore-doped calcium phosphate nanoparticles for in vivo imaging of human breast cancer. *ACS Nano* **2008**, *2*, 2075–2084.

(33) Lee, C. H.; Cheng, S. H.; Wang, Y. J.; Chen, Y. C.; Chen, N. T.; Souris, J.; Chen, C. T.; Mou, C. Y.; Yang, C. S.; Lo, L. W. Near-Infrared Mesoporous Silica Nanoparticles for Optical Imaging: Characterization and In Vivo Biodistribution. *Adv. Funct. Mater.* **2009**, *19*, 215–222.

(34) Kim, T. H.; Chen, Y.; Mount, C. W.; Gombotz, W. R.; Li, X.; Pun, S. H. Evaluation of temperature-sensitive, indocyanine green-encapsulating micelles for noninvasive near-infrared tumor imaging. *Pharm. Res.* **2010**, *27*, 1900–1913.

(35) Kirchherr, A. K.; Briel, A.; Mader, K. Stabilization of indocyanine green by encapsulation within micellar systems. *Mol. Pharmaceutics* **2009**, *6*, 480–491.

(36) Liu, H.; Farrell, S.; Uhrich, K. Drug release characteristics of unimolecular polymeric micelles. *J. Controlled Release* **2000**, *68*, 167–174.

(37) Lavasanifar, A.; Samuel, J.; Kwon, G. S. Poly(ethylene oxide)-block-poly(L-amino acid) micelles for drug delivery. *Adv. Drug Delivery Rev.* **2002**, *54*, 169–190.

(38) Musacchio, T.; Laquintana, V.; Latrofa, A.; Trapani, G.; Torchilin, V. P. PEG-PE micelles loaded with paclitaxel and surface-modified by a PBR-ligand: synergistic anticancer effect. *Mol. Pharmaceutics* **2009**, *6*, 468–479.

(39) Wang, T.; Petrenko, V. A.; Torchilin, V. P. Paclitaxel-loaded polymeric micelles modified with MCF-7 cell-specific phage protein: enhanced binding to target cancer cells and increased cytotoxicity. *Mol. Pharmaceutics* **2010**, *7*, 1007–1014.

(40) Torchilin, V. P. Recent advances with liposomes as pharmaceutical carriers. *Nat. Rev. Drug Discovery* **2005**, *4*, 145–160.

(41) Moghimi, S. M.; Hunter, A. C.; Murray, J. C. Long-circulating and target-specific nanoparticles: theory to practice. *Pharmacol. Rev.* **2001**, *53*, 283–318.

(42) Mosqueira, V. C.; Legrand, P.; Gulik, A.; Bourdon, O.; Gref, R.; Labarre, D.; Barratt, G. Relationship between complement activation, cellular uptake and surface physicochemical aspects of novel PEG-modified nanocapsules. *Biomaterials* **2001**, *22*, 2967–2979.

(43) Basu, S.; Harfouche, R.; Soni, S.; Chimote, G.; Mashelkar, R. A.; Sengupta, S. Nanoparticle-mediated targeting of MAPK signaling predisposes tumor to chemotherapy. *Proc. Natl. Acad. Sci. U.S.A.* **2009**, *106*, 7957–7961.

(44) Ou, Z.; Wu, B.; Xing, D.; Zhou, F.; Wang, H.; Tang, Y. Functional single-walled carbon nanotubes based on an integrin alpha v beta 3 monoclonal antibody for highly efficient cancer cell targeting. *Nanotechnology* **2009**, *20*, 102–105.

(45) Kam, N. W.; Liu, Z.; Dai, H. Carbon nanotubes as intracellular transporters for proteins and DNA: An investigation of the uptake mechanism and pathway. *Angew. Chem., Int. Ed.* **2006**, *45*, 577–581.

(46) Zhou, F.; Xing, D.; Wu, B.; Wu, S.; Ou, Z.; Chen, W. R. New insights of transmembranal mechanism and subcellular localization of noncovalently modified single-walled carbon nanotubes. *Nano Lett.* **2010**, *5*, 1677–1681.

(47) Rodriguez, V. B.; Henry, S. M.; Hoffman, A. S.; Stayton, P. S.; Li, X.; Pun, S. H. Encapsulation and stabilization of indocyanine green within poly(styrene-alt-maleic anhydride) block-poly(styrene) micelles for near-infrared imaging. *J. Biomed. Opt.* **2008**, *13*, 014025.

(48) Muguruma, N.; Ito, S.; Hayashi, S.; Taoka, S.; Kakehashi, H.; Ii, K.; Shibamura, S.; Takesako, K. Antibodies labeled with fluorescence-agent excitable by infrared rays. *J. Gastroenterol.* **1998**, *33*, 467–471.

(49) Tadatsu, Y.; Muguruma, N.; Ito, S.; Tadatsu, M.; Kusaka, Y.; Okamoto, K.; Imoto, Y.; Taue, H.; Sano, S.; Nagao, Y. Optimal labeling condition of antibodies available for immunofluorescence endoscopy. *J. Med. Invest.* **2006**, *53*, 52–60.

(50) Ogawa, M.; Kosaka, N.; Choyke, P. L.; Kobayashi, H. In vivo molecular imaging of cancer with a quenching near-infrared fluorescent probe using conjugates of monoclonal antibodies and indocyanine green. *Cancer Res.* **2009**, *69*, 1268–1272.

(51) Welsher, K.; Liu, Z.; Daranciang, D.; Dai, H. Selective probing and imaging of cells with single walled carbon nanotubes as near-infrared fluorescent molecules. *Nano Lett.* **2008**, *8*, 586–590.

(52) De la Zerda, A.; Liu, Z.; Bodapati, S.; Teed, R.; Vaithilingam, S.; Khuri-Yakub, B. T.; Chen, X.; Dai, H.; Gambhir, S. S. Ultrahigh sensitivity carbon nanotube agents for photoacoustic molecular imaging in living mice. *Nano Lett.* **2010**, *10*, 2168–2172.